ACS APPLIED MATERIALS & INTERFACES

Research Article

www.acsami.org

Graphene Oxide Based Theranostic Platform for T_1-Weighted Magnetic Resonance Imaging and Drug Delivery

Mengxin Zhang,[†,§] Yuhua Cao,[†] Yu Chong,[†] Yufei Ma,[†] Hailu Zhang,*[,‡] Zongwu Deng,[‡] Chunhong Hu,[∥] and Zhijun Zhang*[,†]

[†]Suzhou Key Laboratory of Nanobiomedicine, Division of Nanobiomedicine, Suzhou Institute of Nano-tech and Nano-bionics, Chinese Academy of Sciences, 398 Ruoshui Road, Suzhou 215123, China

[‡]Division of Nanobionics, Suzhou Institute of Nano-tech and Nano-bionics, Chinese Academy of Sciences, 398 Ruoshui Road, Suzhou 215123, China

[§]University of Chinese Academy of Sciences, 19 (A) Yuquan Road, Beijing 100049, China

[∥]Imaging Centre, The First Affiliated Hospital of Soochow University, Suzhou 215006, China

Supporting Information

ABSTRACT: Magnetic resonance imaging (MRI) is a powerful and widely used clinical technique in cancer diagnosis. MRI contrast agents (CAs) are often used to improve the quality of MRI-based diagnosis. In this work, we developed a positive T_1 MRI CA based on graphene oxide (GO)−gadolinium (Gd) complexes. In our strategy, diethylenetriaminepentaacetic acid (DTPA) is chemically conjugated to GO, followed by Gd(III) complexation, to form a T_1 MRI CA (GO−DTPA−Gd). We have demonstrated that the GO−DTPA−Gd system significantly improves MRI T_1 relaxivity and leads to a better cellular MRI contrast effect than Magnevist, a commercially used CA. Next, an anticancer drug, doxorubicin (DOX), was loaded on the surface of GO sheets via physisorption. Thus-prepared GO−DTPA−Gd/DOX shows significant cytotoxicity to the cancer cells (HepG2). This work provides a novel strategy to build a GO-based theranostic nanoplatform with T_1-weighted MRI, fluorescence imaging, and drug delivery functionalities.

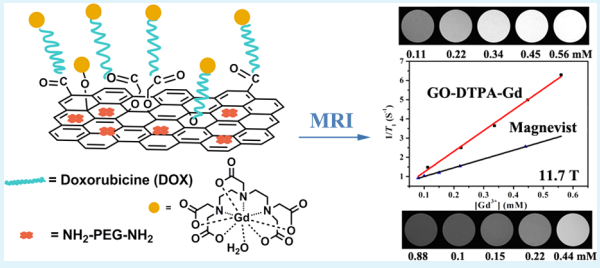

KEYWORDS: *graphene oxide, MR imaging, contrast agents, cellular imaging, theranostics*

INTRODUCTION

Magnetic resonance imaging (MRI) is a powerful and widely used diagnostic technology with high spatial resolution and noninvasiveness and is excellent for imaging soft tissues and organs.[1] However, the innate low sensitivity of MRI often compromises its diagnosis quality. By introduction of MRI contrast agents (CAs), the imaging contrast between normal and pathological sites can be significantly enhanced.[2] Nowadays, approximately one-third of clinical MRI is performed with the assistance of CAs to achieve precise and reliable diagnosis of pathologic changes. MRI CAs can be divided into two types: T_1 and T_2 CAs, depending on the signal enhancement or decay. T_1-weighted CAs can reduce the ^{1}H T_1 relaxation times (spin−lattice relaxation times) of nearby water, resulting in brighter contrast in T_1-weighted images. Gadolinium (Gd) complexes are the frequently employed T_1 CAs for their paramagnetic properties and can effectively increase the proton relaxation rate of water molecules nearby via a dipolar mechanism.[3] T_2-weighted CAs, usually referring to superparamagnetic iron oxide (Fe_3O_4) nanoparticles (NPs), bring darker contrast in T_2-weighted images by reducing the T_2 relaxation times (spin−spin relaxation times).[4] In clinical practice, it is hard to distinguish dark signals of Fe_3O_4 NPs from the blood clots, tissue−air interfaces, and calcification areas, and the MRI signals may extend beyond the volume of the labeled cells for the large magnetic susceptibility of the particles.[5] In this case, T_1 CAs are appreciated for their predominant positive signal enhancement. However, wide application of T_1 MRI CAs in clinics is limited to a large extent, due to their inherent low sensitivity. To improve the relaxivity (r_1), many approaches have been developed, such as designing gadolinium oxide nanocrystals[6] and incorporating the Gd complex with dendrimers, phospholipids, quantum dots, mesoporous silica particles,[7,8] and carbonaceous materials such as fullerene[9−11] and carbon nanotube,[12,13] to modify the molecular parameters that are relevant to the relaxation. Besides, many of the currently existing CAs are restricted to extracellular space[14] and unable to image in the intracellular level. Thus, new MRI CAs with high sensitivity and the ability in cellular imaging are highly desired.

Graphene, a single-layer sheet that has sp^2-bonded carbon atoms, has attracted tremendous interest owing to its

Received: September 30, 2013
Accepted: December 6, 2013
Published: December 6, 2013

Scheme 1. Schematic Illustration of Synthesis of the GO−DTPA−Gd Complex for MR Imaging and Drug Delivery

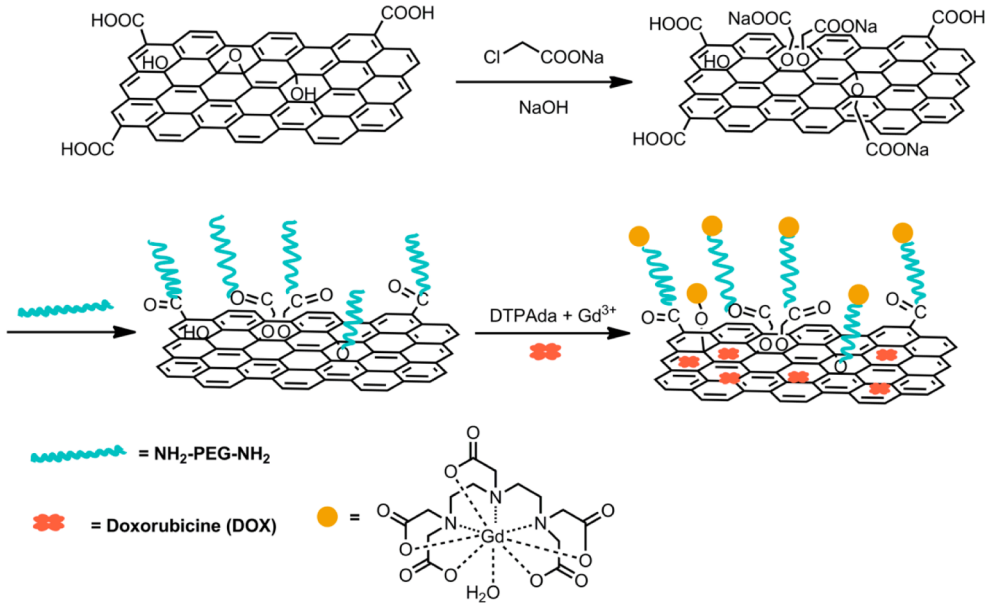

extraordinary electrical, mechanical, thermal, and optical properties.[15−19] Researchers have explored applications of graphene in transparent conductors, energy storage and conversion, nanoelectronics, and field emission display, etc. Great efforts have been devoted recently to explore the application of graphene-based materials in the biomedical field, such as drug delivery, biosensing, cell imaging, and cancer therapies.[20−24] Graphene oxide (GO), one of the most important graphene derivatives, which exhibits excellent water solubility, low toxicity, and ultrahigh specific surface area, is considered as an ideal candidate in biological sensing and imaging and drug delivery.[25,26] It should be noted that though GO is commonly considered safe it may trigger blood platelet.[27] Whereas in the case of PEGylated GO, no obvious toxicity was observed in a long-term (three months) in vivo study,[28] and amine-modified graphene was verified to be relatively safer than GO in animal experiments.[29]

In this work, a versatile theranotic nanoplatform based on GO was built up for MRI and drug delivery. Theranostics, defined as the strategy that combined cancer treatments and diagnosis on a single platform, has attracted increasing interest in the field of nanobiomedicine.[30−32] In our approach, GO was obtained by chemical oxidation of graphite, followed by conjugation with diethylenetriaminepentaacetic acid (DTPA) molecules. Next, Gd^{3+} was complexed to the DTPA ligand, forming GO−DTPA−Gd complexes (Scheme 1). It is expected that the large molecular weight of the GO system can slow down the rotational motion of the water proton, leading to enhanced T_1 relaxivity and imaging contrast, while the large specific surface area of GO allows ultrahigh loading of anticancer drugs. Our results show that GO−DTPA−Gd exhibits significantly improved T_1 relaxivity, being 10.8 mM^{-1} S^{-1}, compared with Magnevist (4.5 mM^{-1} S^{-1}), under 11.7 T. Moreover, in vitro experiment shows that the cellular MRI contrast of HepG2 cells incubated with GO−DTPA−Gd has been significantly enhanced.

EXPERIMENTAL SECTION

Materials and Instruments. The native graphite flake was purchased from Alfa Aesar. Amine polyethylene glycol amine and HCl salt (NH_2−PEG−NH_2, MW 10 000) were obtained from Beijing Jenkem Technology Co., Ltd. Gadolinium(III) chloride hexahydrate was supplied by Sigma-Aldrich. Doxorubicin (DOX) was provided by Shanghai Sangon Co., Ltd. Diethylenetriaminepentaacetic acid dianhydride (DTPAda) was purchased from Aladdin Chemical Co., China. DMEM culture medium and fetal bovine serum were purchased from Invitrogen. WST-1 was purchased from Biyuntian Biotechnology Institute. All other reagents were purchased from China National Medicine Corporation and used without further purification. Ultrapure water (18.2 MΩ·cm) was used throughout the experiments.

Instrument. The GO samples were characterized by a Vecco Dimension 3100 atomic force microscope (AFM) under ambient conditions. Fourier transform infrared (FTIR) spectra of samples (KBr pellet) were collected using a Thermo Nicolet 6700 FTIR spectrometer. Zeta potential was measured by a particle size/zeta analyzer (ZEN3600-nanoZS, Malvern). UV−vis spectra were obtained with a Perkin-Elmer Lambda 25 spectrophotometer. Fluorescence spectra were acquired on a Hitachi F-4600 fluorescence spectrometer. Flow cytometry analysis (FACS) was performed by FACSAria II (Becton Dickinson). Fluorescence imaging was carried out on a Nikon Laser scanning confocal microscope. X-ray photoelectron spectroscopy (XPS) spectra were acquired with a Kratos Axis Ultra^{DLD} spectrometer using a monochromatic Al Kα source at 1486.6 eV. The Gd^{3+} concentration was detected by an inductively coupled plasma atomic emission spectrometer (ICP-AES, Perkin-Elmer Optima 8000). WST assay was conducted using a Biotek Elx 800 Microplate Reader. Cell lines were cultured in a water-jacketed CO_2 incubator (Thermo 3111). MRI was performed on 11.7 T Bruker micro-MRI system with a 25 mm RF coil.

Synthesis of GO. GO was prepared from graphite powder following the protocol described in our previous work.[33] To improve the stability of thus-prepared GO and to facilitate further PEGylation, OH groups on the GO sheets were converted to COOH groups (termed GO−COOH).[20] GO suspension was diluted to give a concentration of about 2 mg/mL. NaOH (5 g) and chloroacetic acid ($ClCH_2COOH$, 5 g) were dissolved in water (20 mL) and then mixed with the GO aqueous solution (30 mL) and kept under bath sonication for 2 h. The resulting GO−COOH solution was neutralized with dilute HCl and purified by repeated rinsing and centrifugation. Then the GO−COOH suspension was dialyzed in distilled water for 3 days to remove impurities.

Synthesis of GO−PEG. For GO PEGylation, aqueous solution GO−COOH (2 mg/mL, 5 mL) was sonicated for 30 min, and the pH was adjusted to 8 with triethylamine. Next, an aqueous solution of

amine−PEG−amine (50 mg/mL, 1 mL) was added under vigorous stirring. An amount of 0.15 mL of EDC at the concentration of 80 mg/mL was added to the solution. After reaction for 30 min, another portion of 0.35 mL of EDC was added and stirred overnight. The final product was dialyzed (MWCO: 100 kDa) against ultrapure water for 48 h to remove unbounded PEG.

Synthesis of GO−DTPA−Gd. GO−PEG−DTPA was synthesized following a modified literature procedure.[34,35] Briefly, DTPAda (0.1 g) and GO−PEG (5 mL) were dissolved in dimethylsulfoxide (DMSO), to which EDC solution (50 mg of EDC in 1 mL of DMSO) and 50 μL of triethylamine were added dropwise and stirred overnight. The product was then dialyzed against ultrapure water for 2 days.

An equivalent volume of $GdCl_3$ solution (20 mM) was added dropwise to the GO−DTPA (for clarity consideration "PEG" was omitted from the acronym in GO−PEG−DTPA) solution, and the mixture was stirred for 4 h, excess $GdCl_3$ was removed by dialysis. The final concentration of Gd^{3+} was determined by ICP-AES.

To investigate its physiological stability, GO−DTPA−Gd was incubated in fetal bovine serum for 24 h. At different time intervals the sample was collected and filtered through a 100 kDa cutoff filter. The percentages of Gd^{3+} remaining on GO−DTPA were calculated according to the following equation[36]

$$\begin{aligned} &Gd^{3+}\text{ complexed to GO−DTPA (\%)} \\ &= (Gd^{3+}\text{ initial concentration} - Gd^{3+}\text{ concentration in filtrate}) \\ &\quad /\text{Gd initial concentration} \times 100 \end{aligned}$$

Loading and Release of Drugs on GO−DTPA−Gd. Loading of anticancer drug DOX can be simply achieved by mixing an aqueous solution of DOX (1 mg/mL) with GO−DTPA−Gd solution. Before drug loading, the pH value of GO−DTPA−Gd solution was adjusted with 0.1 M $NaHCO_3/Na_2CO_3$ buffer. The mixture was agitated magnetically for 4 h in the dark. Free DOX was then removed by dialysis. The concentration of DOX and GO was determined by UV−vis spectroscopy. The concentration of GO was estimated from the absorbance peak at 230 nm. The concentration of DOX adsorbed on GO was calculated from the absorbance peak at 490 nm after subtracting the GO absorbance from that,[37] and the loading ratio refers to the weight ratio of DOX to GO.

The release of DOX from GO−DTPA−Gd was carried out by mixing the material with phosphate buffer solution (PBS) at 37 °C. At a different time point, the mixture was filtered through a 100 kDa cutoff filter. The released drugs were measured by UV−vis spectroscopy.

Cell Culture. Human hepatocellular carcinoma (HepG2) cells were cultured in DMEM growth medium complemented with 10% fetal bovine serum (FBS), streptomycin at 100 μg/mL, and penicillin at 100 units/mL. The cells were maintained at 37 °C in a humidified atmosphere of 5% CO_2 in air.

Cytotoxicity of GO−DTPA−Gd. WST assay was performed to evaluate the toxicity of GO−DTPA−Gd complexes to HepG2 cells. The cells were seeded into 96-well plates at cell density of 5×10^3 cells/well in 180 μL of culture medium and maintained for 24 h. Then 20 μL of GO−DTPA−Gd solution with different Gd^{3+} concentrations was added to 96-well plates and incubated for another 24 or 48 h. The commercially available CA, gadopentetate dimeglumine injection (Gd−DTPA, Magnevist, Bayer HealthCare Pharmaceuticals Inc.), was taken as a control. Finally, the medium was replaced with 100 μL of fresh DMEM, and 10 μL of WST-1 reagent was added to each well. After incubation for 1 h, the absorbance at 450 nm was determined by a standard microplate reader. All experiments were conducted in triplicate. No statistically significant differences were detected.

To study the intracellular delivery behavior of DOX by GO−DTPA−Gd, HepG2 cells were seeded into 96-well plates at a density of 5×10^3 in 180 μL of culture medium and incubated overnight. The culture medium was then added with 20 μL of DOX or GO−DTPA−Gd/DOX at various concentrations (0, 1, 2, and 5 μg/mL in terms of DOX) for another 24 or 48 h. After that, WST-1 assay was performed as described above.

Cellular Uptake of GO−DTPA−Gd. HepG2 cells were seeded into 24-well plates at a density of 1×10^4 cells/well and incubated for 12 h, to which GO−DTPA−Gd/DOX was then added. After further incubation for 2 and 4 h, respectively, the culture medium was washed three times with PBS. The fluorescence images were acquired by confocal laser scanning microscopy with an argon laser at an excitation wavelength of 488 nm, emission wavelength of 570 nm through a filter, field of view (FOV) = 3 × 3 mm, resolution = 1204 × 1204, and number of averages = 2. During the measurement, confocal microscopy settings are held constant.

To quantitate the fluorescence intensity of DOX by cellular uptake, flow cytometry analysis (FACS) was performed. HepG2 cells were seeded into 6-well plates at a density of 2×10^5 cells/well, then incubated with GO−DTPA−Gd/DOX (7.5 μg/mL in terms of DOX) for 2 or 4 h, and collected before measurement. FACS was carried out at an excitation wavelength of 488 nm and an emission wavelength of 570 nm, for 10 000 cells per sample.

MRI Measurements. An 11.7 T MRI scanner was used to measure the T_1 relaxation times of GO−DTPA−Gd aqueous solution at different concentrations. The measurement parameters are as follows: repetition time (TR) = 40, 60, 100, 150, 300, 600, 1000, 2000, 3000, and 5500 ms, echo time (TE) = 7.0 ms, imaging matrix = 128 × 128, slice thickness = 1.2 mm, field of view (FOV) = 2.0 × 2.0 cm, and number of averages (NA) = 2.

To prepare cell MRI phantom, HepG2 cells were seeded into culture dishes at a density of 1×10^6 cells per plate in 10 mL of culture medium and grown overnight. Then, the materials at different concentrations (0, 12.5, 25, and 50 μM Gd^{3+}) were added and incubated for 24 h. Following that, the medium was removed, and the cells were washed in a plate with 5 mL of PBS three times, then digested with trypsin and transferred to a 1.5 mL microcentrifuge tube and collected by centrifugation at 1000 rpm for 5 min. Then the cells were resuspended and washed with 1.5 mL of PBS and collected by centrifugation again. Finally, the cells were dispersed in 1% homogeneous agarose gel and transferred to microtubes for cellular MR imaging. The measurement parameters are as follows: repetition time (TR) = 300.0 ms, echo time (TE) = 5.0 ms, imaging matrix = 128 × 128, slice thickness = 1 mm, field of view (FOV) = 2.0 × 2.0 cm, number of averages (NA) = 4.

RESULTS AND DISCUSSION

Synthesis of GO−DTPA−Gd Complexes. GO was synthesized from graphite powder using the modified Hummer's method. AFM measurement (Figure 1) shows that the average dimension of GO is 100−300 nm, and the thickness of the GO sheet was about 1.0 nm, consistent with that reported previously.[25] After carboxylation of GO, the GO aqueous solution became darker, which was found to be stable at room temperature for more than 8 months. The zeta potential of GO−COOH became more negative, being about −40 mV. This is due to the presence of more carboxylic groups, from the conversion of hydroxyl groups and epoxy groups on the GO surface.

The aqueous solution of GO tends to aggregate in physiological solution such as PBS buffer and cell culture medium. To improve its stability in physiological solutions, GO was conjugated with amino-terminated PEG (NH_2−PEG−NH_2, 10 k) through EDC chemistry.[38] FTIR data show successful PEGlyation of GO (Figure 2). The strong peak around 2890 cm^{-1} is assigned to symmetric and asymmetric stretching modes of methylene ($-CH_2$) groups of PEG. The peak at 1100 cm^{-1} corresponds to the C−O stretching vibration, suggesting conjugation of PEG molecules to the GO sheets.[39] The zeta potential of GO−COOH before and after PEGylation was changed from −40 to −20 mV (Figure S1, Supporting Information), also confirming the attachment of PEG to GO.[40]

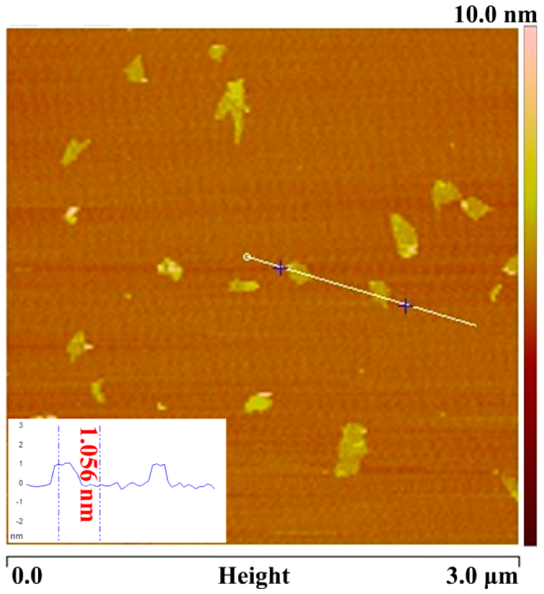

Figure 1. AFM image of GO. The inset shows the average thickness of GO.

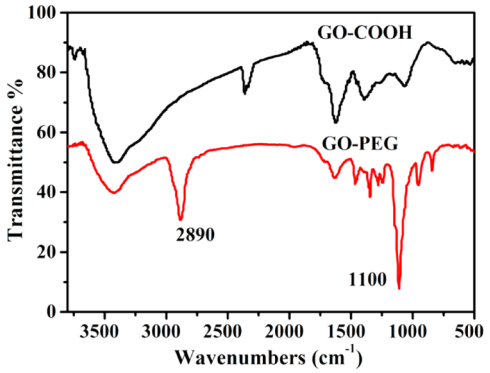

Figure 2. FTIR spectra of GO and GO−PEG (KBr pellet).

Functionalization of GO with DTPA was achieved by chemical reaction between DTPAda and amine groups of GO−PEG. Figure 3 depicts XPS spectra of the N 1s region of GO−PEG before and after being modified with DTPA. The broad, overlapped band can be split into two peaks with binding energies of 399.4 and 400.5 eV by curve fitting. The two peaks can be assigned to amine and amide groups, respectively.[41] Figure 3A and 3B represents N 1s spectra of GO−PEG and GO−PEG−DTPA, respectively. Compared with Figure 3A, it is clear that the amount of amine groups (Figure 3B) increases remarkably. The increase of amine groups can be explained by the presence of N-containing molecules, i.e, DTPA, onto GO−PEG. Thus, this result indicates that DTPA was conjugated onto GO−PEG. Then, by adding Gd^{3+} salt solution to GO−DTPA the GO−DTPA−Gd complexes were formed.

Stability of GO−DTPA−Gd. The biological stability of GO−DTPA−Gd complexes in physiological solution was examined for its importance in biomedical applications. Figure 4A shows that GO−DTPA−Gd is stable in culture medium and fetal bovine serum, while the mixed solution of $Gd^{3+}$and GO−COOH was only stable in water. When added into the culture medium and fetal bovine serum, GO−COOH−Gd aggregated immediately. It clearly reveals that GO−DTPA improves the stability of the complexes in physiological solution. When the

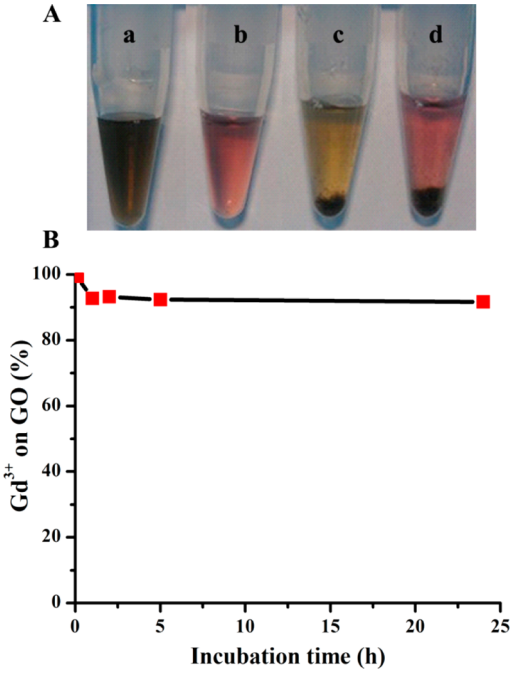

Figure 4. (A) Photograph of GO−DTPA−Gd complexes in (a) fetal bovine serum and (b) cell culture medium and GO−COOH−Gd in (c) fetal bovine serum and (d) cell culture medium. (B) Stability of GO−DTPA−Gd complexes in serum.

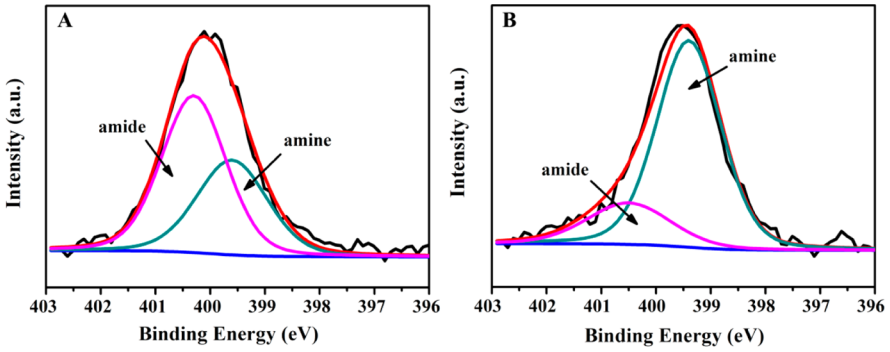

Figure 3. XPS N 1s spectra of GO−PEG (A) and GO−PEG−DTPA (B). The N 1s peak was resolved into two peaks with binding energy at 399.4 and 400.5 eV, respectively.

GO−DTPA−Gd system is incubated with fetal bovine serum, there is more than 90% Gd^{3+} remaining in GO−DTPA after 24 h (Figure 4B). Since T_1 CAs reduce the longitudinal relaxation time through the interaction between Gd^{3+} and water protons, the good stability of the complex of Gd^{3+} to GO−DPTA ensures the enhancement of the MRI signal.

MRI Results. To investigate the MRI contrast enhancement of GO−DTPA−Gd solution, MRI measurement was conducted at an 11.7 T MRI scanner. Figure 5 displays T_1-weighted

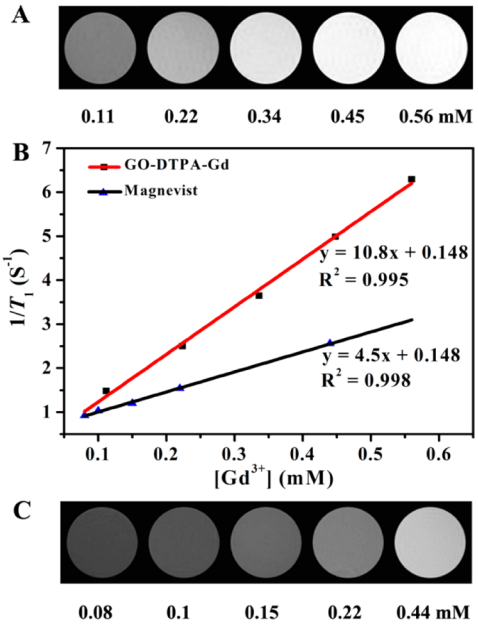

Figure 5. (A) T_1-weighted MR images of GO−DTPA−Gd at different Gd concentrations in water. (B) Plot of relaxation rate r_1 versus Gd^{3+} concentration for GO−DTPA−Gd and Magnevist. The relaxivity value r_1 was obtained from the slope of linear fitting of the experimental data. (C) The T_1-weighted MR images of Magnevist at different Gd concentrations are provided as control.

MR images of GO−DTPA−Gd (Figure 5A) and Magnevist (Figure 5C), respectively. Magnevist, an FDA approved and widely used CA in clinical practice, was chosen as a control. It is clearly evident that MR images enhance with the increase of Gd^{3+} concentration, and GO−DTPA−Gd exhibits much better contrast enhancement and thereby a brighter image than Magnevist.

To quantify the MR signal enhancement, the relaxivity r_1 (mM^{-1} s^{-1}) was calculated. The r_1 is defined as the efficiency of a CA to change the relaxation rate of water protons, which can be calculated from the observed relaxation rate, $1/T_{1,obs}$, by using the equation below

$$1/T_{1,obs} = 1/T_{1,d} + r_1 \times [Gd^{3+}]$$

where $1/T_{1,d}$ is the diamagnetic contribution of water in the absence of paramagnetic species and $[Gd^{3+}]$ is the concentration of Gd^{3+}. The relaxation rate of pure water was taken as the diamagnetic contribution.[13]

Figure 5B shows the relaxation rates of the GO−DTPA−Gd and Magnevist. The r_1 relaxivity was calculated by the linear fit of Gd^{3+}concentration vs $1/T_1$. The r_1 value of GO−DTPA−Gd was determined to be 10.8 mM^{-1} S^{-1}, which is 2.4 times larger than that of Magnevist (4.5 mM^{-1} S^{-1}). The improved relaxivity of GO−DTPA-Gd can be explained by the complexation of Gd to GO−DTPA, which is similar to the conjugation of Gd^{3+} to a macromolecule, leading to slowing molecular tumbling, thus reducing the relaxation time of water.[7] The MRI measurement of GO−COOH solution is shown in Figure S2 (Supporting Information), and its MR signal is rather low (0.249 mM^{-1} s^{-1}).

Fluorescence Imaging. To investigate the cellular uptake behavior of GO−DTPA−Gd complexes, an anticancer drug DOX, which is also a fluorescent dye, was loaded onto the surface of the GO−DTPA−Gd complexes by physisorption. The fluorescence of DOX can be quenched by GO−DTPA−Gd, and the recovery of fluorescence indicates the release of DOX from GO−DTPA−Gd (Figure S3, Supporting Information). By observing the red fluorescence of DOX, the internalized behavior of GO can be monitored.[42] Figure 6 shows that after incubating HepG2 cells with GO−DTPA−Gd for 2 h the red fluorescence of DOX can be detected inside the cells. A longer incubation time (4 h) resulted in a stronger fluorescence signal inside the cells, suggesting more cellular uptake of GO−DTPA−Gd with time. Flow cytometry analysis also exhibits stronger fluorescence intensity of longer incubation time (4 h) than that of 2 h (Figure S4, Supporting Information). Compared with GO−DTPA−Gd/DOX complexes, free DOX diffused into cells rapidly and reached the cell nuclei, showing strong red fluorescence (Figure S5, Supporting Information). The cellular uptake of GO was probably achieved via clathrin-mediated, energy-dependent endocytosis, as was reported by us previously.[43] Moreover, the observation of strong red fluorescence of the GO−DTPA−Gd/DOX system inside the cells implies that this MRI CA can also be employed for fluorescence imaging, which could provide additional information complementary to cellular MR imaging for optimal diagnosis.

Cellular MRI. As discussed above, the GO−DTPA−Gd complexes exhibit much higher relaxivity than Magnevist in aqueous solution and can be uptaken efficiently by HepG2 cells. The intracellular MRI using GO−DTPA−Gd was then investigated by incubation of HepG2 cells with the GO−DTPA−Gd complexes at different Gd concentrations. Figure 7 presents T_1-weighted MRI of HepG2 cells. Under the same Gd^{3+} concentration, the GO−DTPA−Gd system shows much brighter MRI contrast (Figure 7e) for labeling HepG2 cells than Magnevist (Figure 7b). With the increase of Gd^{3+} concentration of GO−DTPA−Gd, from 0, 12.5, 25, to 50 μM, respectively, the cellular MRI signal enhanced gradually (Figure 7a, 7c, to 7e). Generally the cellular MR imaging quality of Gd-based CA is limited because small Gd complex molecules, such as Magnevist, tend to distribute in the extracellular space. One of the useful strategies to solve this problem is to adopt nanosized carriers to deliver a large number of paramagnetic metal complexes to improve the MRI contrast of labeled cells.[14] Currently, cell labeling is mainly accomplished by endocytosis of iron oxide particles as T_2 negative CAs. Our results demonstrated that the nanosized GO−DTPA−Gd complexes can be internalized into cells and exhibit good T_1 MRI contrast in cellular imaging. Our current study is limited at the cellular level, and further work at the in vivo level is highly desired for practical application of the GO−DTPA−Gd. To target a specific site in animal studies, a small molecular ligand, such as lactobionic acid and folic acid, both of which contain a carboxyl moiety, can be used to conjugate amino-terminated PEG on GO sheets.

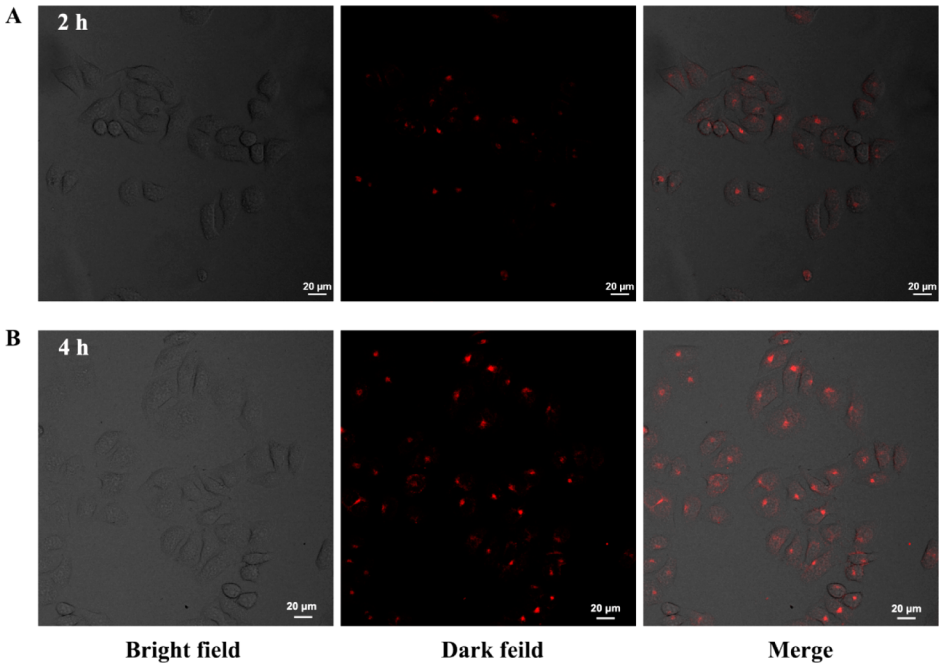

Figure 6. Confocal fluorescence microscopic images of HepG2 cells incubated with GO−DTPA−Gd/DOX at 37 °C for (A) 2 h and (B) 4 h, respectively. Scale bar: 20 μm.

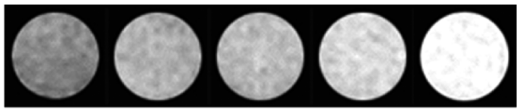

Figure 7. T_1-weighted cellular MR images of agar phantoms. HepG2 cells as control group. HepG2 cells were incubated with Magnevist (50 μM) and GO−DTPA−Gd at a Gd^{3+} concentration of 12.5, 25, and 50 μM, respectively.

Cytotoxicity of GO−DTPA−Gd and GO−DTPA−Gd/DOX. For biomedical applications such as drug delivery and cellular imaging, the toxicity of drug carriers or imaging agents is a priority consideration. To evaluate the cytotoxicity of the GO−DTPA−Gd complexes, WST assay was performed with HepG2 cell lines. When incubated with GO−DTPA−Gd for 24 h, the cell viability was more than 90% with Gd^{3+} concentration up to 50 μM, comparable to that of Magnevist at the same concentration (Figure 8A). A longer incubation time (48 h) did not increase the cytotoxicity significantly (Figure 8B), suggesting the low cytotoxicity of the GO−DTPA−Gd complexes.

DOX, a typical anticancer drug, can be simply adsorbed on the surface of GO−DTPA−Gd to build up a theranostic nanoplatform. After mixing GO−DTPA−Gd with DOX, the color of the solution became red, and the appearance of an absorption peak at 490 nm in the UV−vis spectrum (Figure 9A) indicates that DOX has been successfully adsorbed onto the surface of GO. The drug loading ratio was determined to be 70% (the weight ratio of DOX to GO).

To demonstrate that the intracellular delivery of DOX is pharmacologically active, HepG2 cells were treated with GO−DTPA−Gd/DOX complexes. As shown in Figure 9B, after incubating with cells for 24 h, the GO−DTPA−Gd/DOX complexes did not exhibit noticeable cytotoxicity, with the relative cell viability about 80%. When increasing the incubation time to 48 h, the cell viability decreases to less than 50% at the DOX concentration of 5 μg/mL. The release of DOX is a sustained process and can be facilitated in acidic condition.[37] In the release study of DOX, about 30% DOX was released after

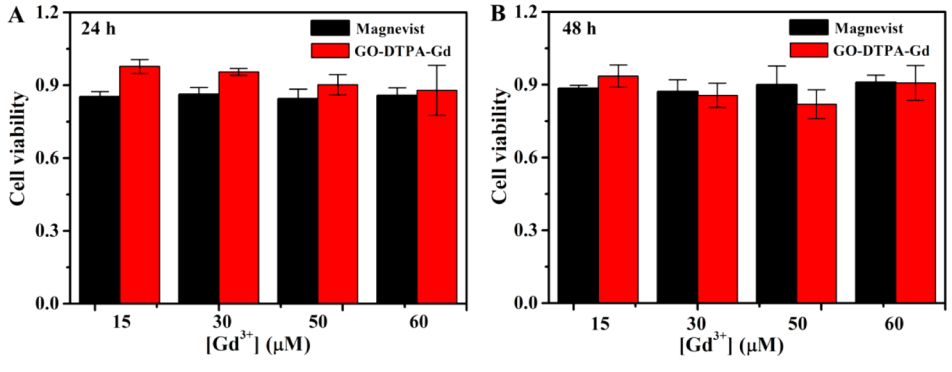

Figure 8. Relative viability of HepG2 cells incubated with GO−DTPA−Gd and Magnevist at different Gd^{3+} concentrations for 24 and 48 h, respectively. Error bars in (A) and (B) were based on triplicate samples.

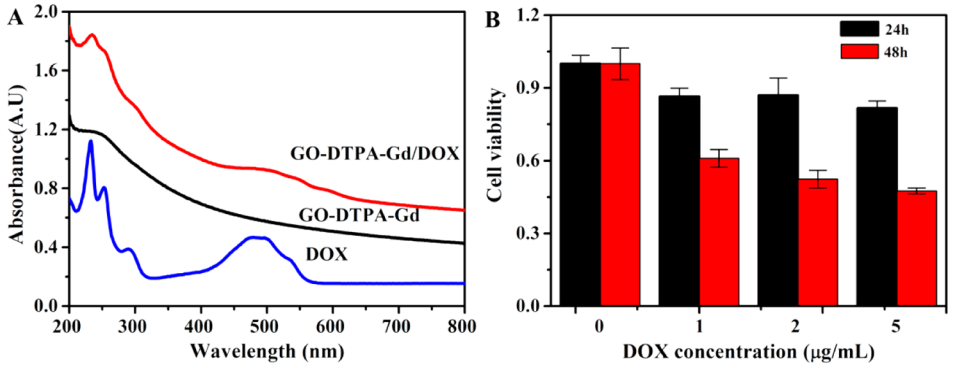

Figure 9. (A) UV/vis spectra of GO−DTPA−Gd, DOX, and GO−DTPA−Gd/DOX. (B) Relative viability of HepG2 cells treated with GO−DTPA−Gd/DOX at different DOX concentrations for 24 and 48 h, respectively. Error bars in (A) and (B) were based on triplicate samples.

48 h in phosphate buffer at pH 5.4, while at pH 7.2 much less DOX was released after 48 h (Figure S6, Supporting Information). The microenvironments of tumor tissues and cell organelles such as lysosomes and endosomes are acidic,[20] and after incubation for 48 h, it can be speculated that sufficient DOX was released from the GO surface and entered the nucleus, resulting in killing of cancer cells.

CONCLUSIONS

In summary, we have developed a GO−DTPA−Gd/DOX-based theranostic nanoplatform with dual modality T_1 MRI/fluorescence imaging and drug delivery functionalities. The GO−DTPA−Gd complexes are physiologically stable and exhibit low cytotoxicity. For T_1-weighted MR imaging, GO−DTPA−Gd complexes exhibit significantly higher r_1 relaxivity enhancement than the commercially used Magnevist, being 2.4 times at 11.7 T. Particularly, the MRI CA developed by us can be internalized into cells and is capable of cellular MR imaging. Moreover, GO−DTPA−Gd complexes show high drug loading capacity (70%) for DOX. The DOX-loaded GO−DTPA−Gd system presents significant cytotoxicity against HepG2 cells. Taking together, this work provides a new, efficient strategy to construct a GO-based theranostic nanoplatform for simultaneous multimodal T_1-weighted MR/fluorescence imaging and therapeautics.

ASSOCIATED CONTENT

Supporting Information

Zeta potential distribution, relaxation rate of GO−COOH, fluorescence emission spectra and flow cytometry analysis GO−DTPA−Gd/DOX, confocal fluorescence microscopic images, and release behavior of DOX. This material is available free of charge via the Internet at http://pubs.acs.org.

AUTHOR INFORMATION

Corresponding Authors

*Tel.: 86-512-62872713. E-mail: hlzhang2008@sinano.ac.cn (H. Zhang).

*Tel.: 86-512-62872556. E-mail: zjzhang2007@sinano.ac.cn (Z. Zhang).

Notes

The authors declare no competing financial interest.

ACKNOWLEDGMENTS

We greatly acknowledge financial support from National Natural Science Foundation of China (Grant Nos. 51361130033, 21205129, 81171393, 31271066). The MRI system used in this study was funded through the key scientific equipment plan of the Chinese Academy of Sciences.

REFERENCES

(1) Chaughule, R. S.; Purushotham, S.; Ramanujan, R. V. *Proc. Natl. Acad. Sci., India, Sect. A* **2012**, *82*, 257−268.
(2) Zhou, Z. X.; Lu, Z. R. *Wiley Interdiscip. Rev. Nanomed. Nanobiotechnol.* **2013**, *5*, 1−18.
(3) Caravan, P.; Ellison, J. J.; McMurry, T. J.; Lauffer, R. B. *Chem. Rev.* **1999**, *99*, 2293−2352.
(4) Laurent, S.; Forge, D.; Port, M.; Roch, A.; Robic, C.; Elst, L. V.; Muller, R. N. *Chem. Rev.* **2008**, *108*, 2064−2110.
(5) Letourneau, M.; Tremblay, M.; Faucher, L.; Rojas, D.; Chevallier, P.; Gossuin, Y.; Lagueux, J.; Fortin, M. A. *J. Phys. Chem. B* **2012**, *116*, 13228−13238.
(6) Ma, X. H.; Gong, A.; Xiang, L. C.; Chen, T. X.; Gao, Y. X.; Liang, X. J.; Shen, Z. Y.; Wu, A. G. *J. Mater. Chem. B* **2013**, *1*, 3419−3428.
(7) Cheng, Y. Y.; Zhao, L. B.; Li, Y. W.; Xu, T. W. *Chem. Soc. Rev.* **2011**, *40*, 2673−2703.
(8) Botta, M.; Tei, L. *Eur. J. Inorg. Chem.* **2012**, 1945−1960.
(9) Mikawa, M.; Kato, H.; Okumura, M.; Narazaki, M.; Kanazawa, Y.; Miwa, N.; Shinohara, H. *Bioconjugate Chem.* **2001**, *12*, 510−514.
(10) Bolskar, R. D.; Benedetto, A. F.; Husebo, L. O.; Price, R. E.; Jackson, E. F.; Wallace, S.; Wilson, L. J.; Alford, J. M. *J. Am. Chem. Soc.* **2003**, *125*, 5471−5478.
(11) Zhen, M. M.; Zheng, J. P.; Ye, L.; Li, S. M.; Jin, C.; Li, K.; Qiu, D.; Han, H. B.; Shu, C. Y.; Yang, Y. J.; Wang, C. R. *ACS Appl. Mater. Interfaces* **2012**, *4*, 3724−3729.
(12) Sitharaman, B.; Kissell, K. R.; Hartman, K. B.; Tran, L. A.; Baikalov, A.; Rusakova, I.; Sun, Y.; Khant, H. A.; Ludtke, S. J.; Chiu, W.; Laus, S.; Toth, E.; Helm, L.; Merbach, A. E.; Wilson, L. J. *Chem. Commun.* **2005**, 3915−3917.
(13) Hartman, K. B.; Laus, S.; Bolskar, R. D.; Muthupillai, R.; Helm, L.; Toth, E.; Merbach, A. E.; Wilson, L. J. *Nano Lett.* **2008**, *8*, 415−419.
(14) Gianolio, E.; Stefania, R.; Di Gregorio, E.; Aime, S. *Eur. J. Inorg. Chem.* **2012**, *2012*, 1934−1944.
(15) Geim, A. K.; Novoselov, K. S. *Nat. Mater.* **2007**, *6*, 183−191.
(16) Neto, A. C.; Guinea, F.; Peres, N.; Novoselov, K.; Geim, A. *Rev. Mod. Phys.* **2009**, *81*, 109−162.
(17) Schwierz, F. *Nat. Nanotechnol.* **2010**, *5*, 487−496.
(18) Chen, D.; Tang, L. H.; Li, J. H. *Chem. Soc. Rev.* **2010**, *39*, 3157−3180.
(19) Sun, Y. Q.; Wu, Q. O.; Shi, G. Q. *Energy Environ. Sci.* **2011**, *4*, 1113−1132.
(20) Sun, X. M.; Liu, Z.; Welsher, K.; Robinson, J. T.; Goodwin, A.; Zaric, S.; Dai, H. J. *Nano Res.* **2008**, *1*, 203−212.
(21) Pan, Y. Z.; Sahoo, N. G.; Li, L. *Expert Opin. Drug Delivery* **2012**, *9*, 1365−1376.

(22) Shen, H.; Zhang, L. M.; Liu, M.; Zhang, Z. J. *Theranostics* **2012**, *2*, 283−294.
(23) Feng, L. Z.; Liu, Z. *Nanomedicine* **2011**, *6*, 317−324.
(24) Shen, A. J.; Li, D. L.; Cai, X. J.; Dong, C. Y.; Dong, H. Q.; Wen, H. Y.; Dai, G. H.; Wang, P. J.; Li, Y. Y. *J. Biomed. Mater. Res. A* **2012**, *100*, 2499−2506.
(25) Liu, Z.; Robinson, J. T.; Sun, X. M.; Dai, H. J. *J. Am. Chem. Soc.* **2008**, *130*, 10876−10877.
(26) Zhang, L. M.; Lu, Z. X.; Zhao, Q. H.; Huang, J.; Shen, H.; Zhang, Z. J. *Small* **2011**, *7*, 460−464.
(27) Singh, S. K.; Singh, M. K.; Nayak, M. K.; Kumari, S.; Shrivastava, S.; Grácio, J. J.; Dash, D. *ACS Nano* **2011**, *5*, 4987−4996.
(28) Yang, K.; Wan, J.; Zhang, S.; Zhang, Y.; Lee, S. T.; Liu, Z. *ACS Nano* **2010**, *5*, 516−522.
(29) Singh, S. K.; Singh, M. K.; Kulkarni, P. P.; Sonkar, V. K.; Grácio, J. J.; Dash, D. *ACS Nano* **2012**, *6*, 2731−2740.
(30) Janib, S. M.; Moses, A. S.; MacKay, J. A.; Ad Zhang, L. M. *Drug Delivery Rev.* **2010**, *62*, 1052−1063.
(31) Kelkar, S. S.; Reineke, T. M. *Bioconjugate Chem.* **2011**, *22*, 1879−1903.
(32) Choi, K. Y.; Liu, G.; Lee, S.; Chen, X. Y. *Nanoscale* **2012**, *4*, 330−342.
(33) Zhang, L. M.; Xia, J. G.; Zhao, Q. H.; Liu, L. W.; Zhang, Z. J. *Small* **2010**, *6*, 537−544.
(34) Chen, Z. J.; Yu, D. X.; Liu, C. X.; Yang, X. Y.; Zhang, N.; Ma, C. H.; Song, J. B.; Lu, Z. J. *J. Drug Targeting* **2011**, *19*, 657−665.
(35) Liu, Y. J.; Zhang, N. *Biomaterials* **2012**, *33*, 5363−5375.
(36) Hong, H.; Zhang, Y.; Engle, J. W.; Nayak, T. R.; Theuer, C. P.; Nickles, R. J.; Barnhart, T. E.; Cai, W. B. *Biomaterials* **2012**, *33*, 4147−4156.
(37) Sherlock, S. P.; Tabakman, S. M.; Xie, L. M.; Dai, H. J. *ACS Nano* **2011**, *5*, 1505−1512.
(38) Wu, L.; Wang, J. S.; Feng, L. Y.; Ren, J. S.; Wei, W. L.; Qu, X. G. *Adv. Mater.* **2012**, *24*, 2447−2452.
(39) Zhang, L. M.; Wang, Z. L.; Lu, Z. X.; Shen, H.; Huang, J.; Zhao, Q. H.; Liu, M.; He, N. Y.; Zhang, Z. J. *J. Mater. Chem. B* **2013**, *1*, 749−755.
(40) Shen, H.; Liu, M.; He, H. X.; Zhang, L. M.; Huang, J.; Chong, Y.; Dai, J. W.; Zhang, Z. J. *ACS Appl. Mater. Interfaces* **2012**, *4*, 6317−6323.
(41) Yang, X. M.; Tu, Y. F.; Li, L.; Shang, S. M.; Tao, X. M. *ACS Appl. Mater. Interfaces* **2010**, *2*, 1707−1713.
(42) Huang, J.; Zong, C.; Shen, H.; Cao, Y. H.; Ren, B.; Zhang, Z. J. *Nanoscale* **2013**, *5*, 10591−10598.
(43) Huang, J.; Zong, C.; Shen, H.; Liu, M.; Chen, B.; Ren, B.; Zhang, Z. J. *Small* **2012**, *8*, 2577−2584.